Materials Research, Vol. 5, No. 4, 427-432, 2002.

Homogeneous Gaussian Profile P^+-Type Emitters: Updated Parameters and Metal-Grid Optimization

M. Cid, N. Stem*

Laboratório de Microeletrônica – Depto. de Engenharia de Sistemas Eletrônicos
Escola Politécnica da Universidade de São Paulo
C.P. 61548, 05424-970 São Paulo - SP, Brazil

Received: May 4, 2001; Revised: April 16, 2002

P^+-type emitters were optimized keeping the base parameters constant. Updated internal parameters were considered. The surface recombination velocity was considered variable with the surface doping level. Passivated homogeneous emitters were found to have low emitter recombination density and high collection efficiency. A complete structure p^+nn^+ was analyzed, taking into account optimized shadowing and metal-contacted factors for laboratory cells as function of the surface doping level and the emitter thickness. The base parameters were kept constant to make the emitter characteristics evident. The most efficient P^+-type passivated homogeneous emitters, provide efficiencies around 21% for a wide range of emitter sheet resistivity (50 – 500 Ω/□) with the surface doping levels $N_s = 1 \times 10^{19}$ cm^{-3} and 5×10^{19} cm^{-3}. The output electrical parameters were evaluated considering the recently proposed value $n_i = 9.65 \times 10^9$ (cm^{-3}). A non-significant increase of 0.1% in the efficiency was obtained, validating all the conclusions obtained in this work, considering $n_i = 1 \times 10^{10}$ cm^{-3}.

Keywords: *theoretical optimization, homogeneous passivated emitters, p^+-type, Gaussian profile, metal-grid*

1. Introduction

It is well-known that some effects such as band gap narrowing, Fermi level degeneracy and changes on behavior of minority carrier lifetime and mobility occur when a region is highly doped, as for solar cell emitters. Many theoretical optimizations have been made taking these effects into account[1,2]. According to these theoretical predictions the best p^+-type passivated homogeneous emitters were found to have surface doping level $N_s = 1 \times 10^{19}$ cm^{-3} and thickness $W_e = 4$ μm, for conventional cells with finger width of 100 μm.

Traditionally, the passivated emitter surface recombination velocity has been considered constant $S_p = 1640$ cm/s. Recently, A. Cuevas *et al.*[3] showed the dependence of the surface recombination velocity on the surface doping level, making new optimizations imperative.

In this work, theoretical models with analytical solutions have been used to study p^+ emitter regions. The recombination and collection efficiency are written as function of series of multiple integrals and in order to assure good accuracy, a fifth order approximation was considered. A simulator code was developed to optimize each particular region of the solar cell (emitter, base and n^+ region) and the complete structure p^+nn^+. In this code a Gaussian profile was chosen and the passivated homogeneous emitters were optimized. Emitters had the recombination current density and efficiency collection calculated as function of the surface doping level and sheet resistivity, considering passivated region surface recombination velocity variable[3]. The surface recombination velocity was kept constant for metal contacted region, $S_n = 3 \times 10^6$ cm/s.

To calculate theoretical solar cell efficiency, a complete p^+nn^+ structure was considered. The base region was assumed to have 300 μm thickness and resistivity of 2.3 Ω.cm. The lifetime was assumed to be 1.5 ms[4]. In order to make the emitter influence evident, the rear surface recombination velocity and the base recombination current density were assumed to be null. Neither light trapping effects and nor surface reflection have been taken into account. The short-circuit current density was obtained adopting the standard spectrum AM1.5G (ASTM892-87) and updated optical absorption coefficients[5].

The metal-grid optimization was carried out using the

*e-mail: nstem@lme.usp.br

traditional expressions to calculate the power loss[6] and considering typical laboratory solar cells with Ti-Pd-Ag contacts with finger width of 5 μm and 30 μm before and after electroplating, respectively.

The shadowing factor, F_s, and the metal grid factor, F_m, were optimized as function of the emitter sheet resistivity and the correspondent metal-semiconductor contact resistivity. The metal-semiconductor contact resistivity dependence on surface doping level was extracted from Swirhun curves[7]. An interactive process was adopted and the optimum shadowing factor for each surface doping level was obtained when the normalized total loss power (grid loss power, contact metal-semiconductor loss power and loss power due to the lateral current flow in the emitter) became equal to the shadowing loss, assuring an accuracy of 0.1%. The metal sheet resistivity (Ag) was assumed to be constant, $\rho_c \approx 2\ m\Omega$[8]. In order to make evident the emitter characteristics, the base loss power was assumed to be null.

Thus, the optimum metal-contacted factor, F_m, was calculated taking into account the optimum shadowing factor, F_s, for each surface doping level according to Eq. 1.

$$F_m = (17\%)\ x\ F_s \quad (1)$$

The output parameters (short-circuit current density, J_{sc}, open-circuit voltage, V_{oc} and efficiency, η) and the intrinsic fill factor, FF_O were calculated using well-known relationships[6]. The final fill factor, FF presented in Eq. 2 takes into account the optimum normalized grid loss power, P_t and the intrinsic fill factor, FF_O.

$$FF = (1 - P_t) \times FF_O \quad (2)$$

2. Updated Internal Parameters and Expressions

Table 1 shows the expressions and the internal parameters that were adopted in this work. It can be observed that the intrinsic concentration was assumed to be 1×10^{10} cm^{-3} and an updated surface recombination velocity was considered dependent on surface doping level for passivated region[3].

All the calculations in this work were made adopting $n_i = 1 \times 10^{10}$ cm^{-3}, despite the recent change[9] to $n_i = 9.65 \times 10^9$ cm^{-3} [9], since the former is still the most accepted in the scientific community.

Although initially developed for the outdated value of $n_i = 1.45 \times 10^{10}$ cm^{-3}, the minority carrier mobility and band gap narrowing expressions[2] presented in Table 1 keep on being the best fitting to the experimental results. These empirical expressions were obtained with the PCD technique, by the measurement of the reason J_o/n_i^2. Therefore, a change of n_i only interferes in the obtained J_o and not in the reason J_o/n_i^2. Thus, the minority carrier mobility and the band gap narrowing expressions are independent on n_i. This conclusion is quite important, because it validates the expressions presented in Table 1 for both $n_i = 1 \times 10^{10}$ cm^{-3} and the recently proposed $n_i = 9.65 \times 10^9$ cm^{-3} (for 300 K).

Table 1. Internal parameters and expressions for p$^+$-type silicon.

$T = 300K,\ n_i = 1\times10^{10}\ (cm^{-3})$
$\tau_n^{-1} = 1\times10^{-31} N_a^{\ 2}\ (s^{-1})$
$\mu_n = 232 + \frac{1180}{1+\left(\frac{N_a}{8.3\times10^{16}}\right)^{0.9}}\ (cm^2/V.s)$
$\Delta E_{gap} = 0.0178\left(\ln\left(\frac{N_a}{2.3\times10^{17}}\right)\right)\ (eV) \quad 10^{18}(cm^{-3}) - 1 < N_a < 10^{21}(cm^{-3})$
$S_n = 500\left(\frac{N_a}{10^{16}}\right)^{\frac{1}{3}}\ (cm/s) \quad 10^{16}(cm^{-3}) < N_a < 10^{20}(cm^{-3})$ (passivated region)
$S_n = 3\times10^6\ (cm/s)$ (metal − contacted region)

3. Emitter Optimization

3.1. Recombination

Figure 1 shows current densities for two kinds of regions (metal-contacted and passivated) as function of emitter sheet resistivity, $R_\square$ and doping level, N_s, considering their respective surface recombination velocities, $S_p = 3 \times 10^6$ cm/s and $S_p = 500\ (Na/10^{16})^{1/3}$ cm/s.

It can be observed that for metal-contacted regions the recombination current density decreases as the surface doping level and the emitter sheet resistivity increase (corresponding to shallower emitters). Therefore, the best recombination current densities are found for thick and highly doped emitters.

However, for the passivated region the lowest recombination current densities were found for low surface doping levels ($N_s = 5 \times 10^{18}$ cm^{-3} and 1×10^{19} cm^{-3}), being practically constant as emitter sheet resistivity increases. It can be observed that highly doped emitters present lower recombination than passivated emitters when a low emitter sheet resistivity is considered.

Thus, in order to evaluate the contributions of the metal-contacted and passivated regions to the total recombination (J_{oe}), the surface doping level $N_s = 1 \times 10^{19}$ cm^{-3} was chosen, due to lower metal-semiconductor contact resistivity. To calculate the components, it was taken into account the occupation area of both kinds of regions, metal-contacted and passivated, multiplying the components by the weight

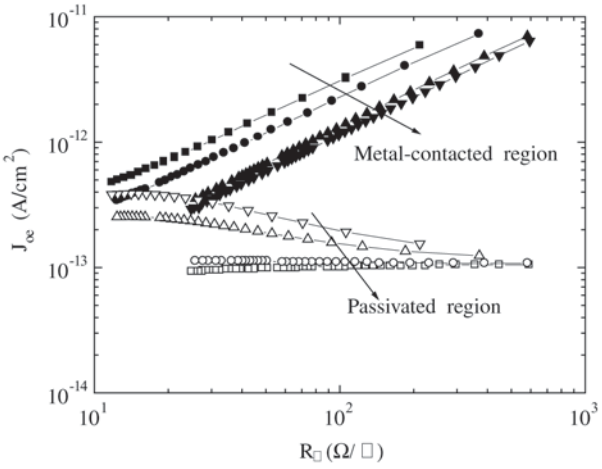

Figure 1. The total emitter recombination current density, J_{oe} as function of emitter sheet resistivity, $R_{\square}$ and surface doping level, N_s, considering two different regions metal-contacted ($S_p = 3\times10^6$ cm/s) and passivated regions ($S_p = 500\ (Na/10^{16})^{1/3}$ cm/s). Metal-contacted region: -■- $N_s = 5\times10^{18}$ (cm^{-3}), -●- $N_s = 1\times10^{19}$ (cm^{-3}), -▲- $N_s = 5\times10^{19}$ (cm^{-3}) and -▼- $N_s = 1\times10^{20}$ (cm^{-3}). Passivated region: -▽- $N_s = 1x10^{20}$ (cm^{-3}), -△- $N_s = 5\times10^{19}$ (cm^{-3}), -○- $N_s = 1\times10^{19}$ (cm^{-3}) and -□- $N_s = 5\times10^{18}$ (cm^{-3}).

factors, F_m and $(1\text{-}F_m)$, respectively, as it can be seen in equation (3).

$$J_{oe} = (1 - F_m)\times J_{pass} + F_m \times J_{met} \quad (3)$$

Figure 2 shows the total emitter recombination current density, J_{oe}, and its components, the passivated, J_{pass}, and the metal-contacted, J_{met}, region recombination current densities versus emitter thickness, W_e, considering $N_s = 1 \times 10^{19}$ cm^{-3}.

In this figure, it can be observed that the passivated component presents a larger contributition than the metal-contacted one, due the difference found in the weight factors of both in Eq. 3.

To make a more detailed evaluation of the total recombination current density behavior, each emitter region recombination current density (metal-contacted, J_{met}, and passivated, J_{pass}) was divided into two components: volume recombination, J_{vol} and surface recombination, J_s, as it can be seen in Figs. 3 and 4.

According to Figs. 3 and 4 the surface recombination current density, J_s, is the major contributor to the recombination of both regions (metal-contacted, J_{met}, and passivated, J_{pass}) about 99.6% and 94.6%, respectively.

However, in Fig. 3, it can be seen in the metal-contacted region that the volume recombination, J_{vol}, is practically constant as the emitter thickness increases, while if it is

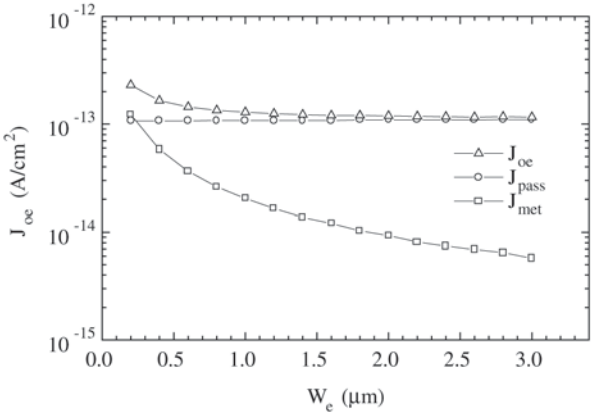

Figure 2. The total emitter recombination current density, J_{oe} and the components passivated and metal contacted region recombination current densities, J_{pass} and J_{met} respectively, as function of emitter thickness, considering the surface doping level $N_s=1\times10^{19}$ cm^{-3} and taking into account the correspodent weight factors $(1\text{-}F_m)$ and F_m , accordingly Eq. 3.

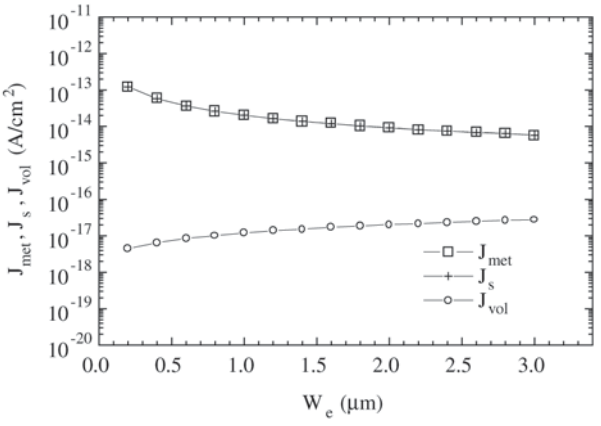

Figure 3. The metal-contacted recombination current density, J_{met} and the components surface and volume recombination density, J_s and J_{vol} respectively versus emitter thickness, W_e, considering $N_s=1\times10^{19}$ cm^{-3} and taking into account the weight factor F_m.

compared to Fig. 4, for passivated region, a more significant contribution of this component is found. In the latter figure the volume recombination increases the contribution about 10 times as the emitter thickness increases from 0.2 to 3.4 μm.

3.2. Emitter collection efficiency

Figure 5 shows a comparison between the emitter collection efficiency as function of emitter sheet resistivity and surface doping level, considering homogeneous passivated emitters.

According to this figure, the highly doped emitter col-

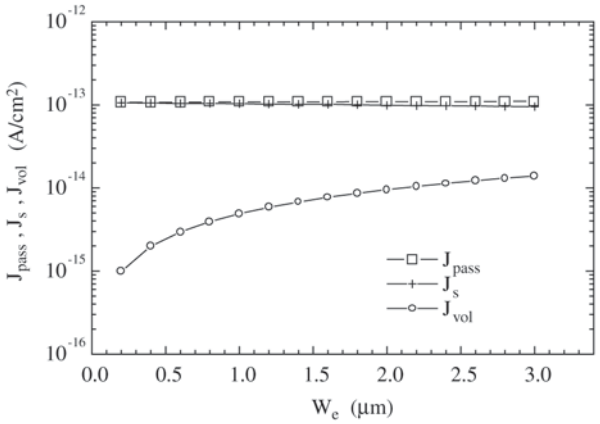

Figure 4. The passivated recombination current density, J_{pass} and the components surface and volume recombination current density as function of emitter thickness, J_s and J_{vol} respectively, considering N_s=1×10^{19} cm^{-3} and taking into account the weight factor (1-F_m).

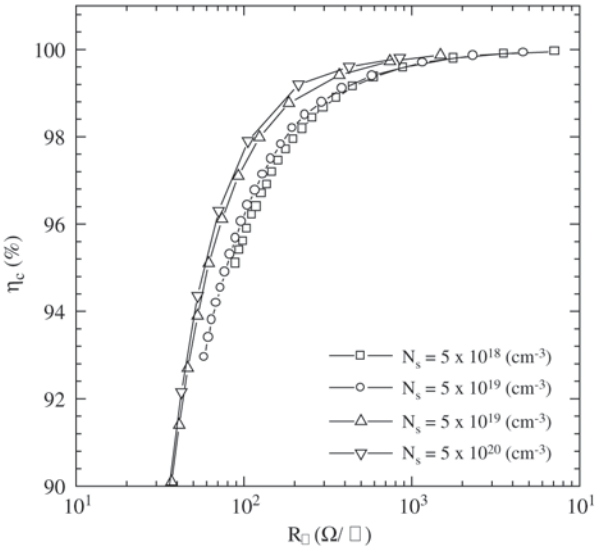

Figure 5. Emitter collection efficiency, η_c as function of emitter sheet resistivity, $R_\square$ and surface doping level, N_s, considering passivated surfaces.

lection effciencies are higher than the moderately doped ones since the same value of emitter sheet resistivity is considered. However, when optimized emitters are focused, the moderately doped emitters present slightly higher efficiencies. Thus, analyzing the optimum short-circuit current densities in Fig. 6 for each surface doping level case, it can be found that the moderately doped emitters present the highest optimum emitter sheet resitivities (the thickest optimized emitters). For instance, chosing the optimum sheet resistivies from Fig. 6 curves, it can be seen in Fig. 5 that the optimized collection efficencies for N_s=5×10^{18} cm^{-3} and

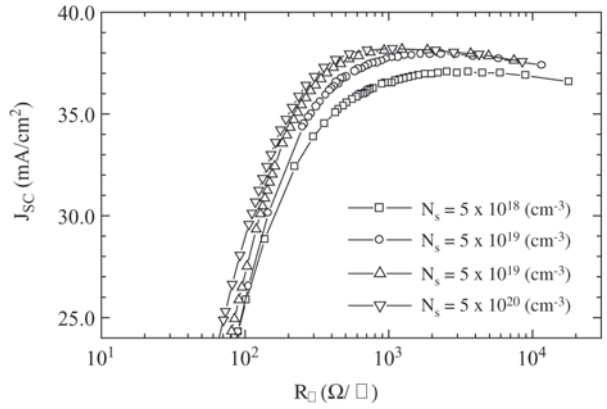

Figure 6. Short-circuit current density, J_{sc} as function of emitter sheet resistivity, $R_\square$ and surface doping level, N_s, considering p-type emitter solar cells.

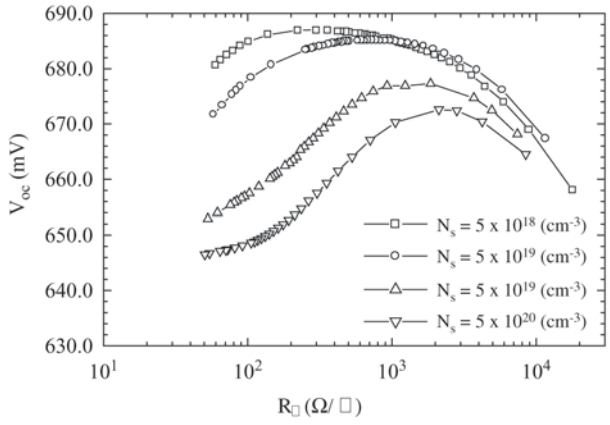

Figure 7. Open circuit voltage, V_{oc} as function of emitter sheet resistivity, $R_\square$ and surface doping level, N_s, considering p-type emitter solar cells.

N_s=1x10^{20} cm^{-3} cases are quite close η_c = (98.4 – 97.9)% with their correspondent sheet resistivities (255-106) Ω/□.

One point to be stressed is that such close values are not found when the respective short-circuit current densities are calculated as it can be seen in Fig. 6. In these curves, the maximum short-circuit current densities are quite different when compared moderately and highly doped emitters, N_s = 5×10^{18} cm^{-3} and N_s = 1×10^{20} cm^{-3}, respectively. This difference is attributed to the metal-grid shadowing factor (1-F_s) influence.

4. A Complete Structure: P$^+$NN$^+$ Solar Cells

In order to compare the emitter effects on the complete structure P$^+$nn$^+$, the base and n$^+$ regions have been considered constant. The recombination current density of base

Table 2. Comparison of the electrical output parameters (J_{sc}, V_{oc}, FF e η), considering $n_i = 1 \times 10^{10}$ cm^{-3} and the newest $n_i = 9.65 \times 10^9$ cm^{-3}, for optimized emitters.

N_s (cm^{-3})	W_e (μm)	$n_i = 1\times 10^{10}$ cm^{-3}				$n_i = 9.65 \times 10^9$ cm^{-3}			
		J_{sc} (mA/cm^2)	V_{oc} (mV)	FF	η (%)	J_{sc} (mA/cm^2)	V_{oc} (mV)	FF	η (%)
5 x 10^{18}	1.4	37.0	681.2	0.792	20.0	37.0	683.0	0.793	20.1
1 x 10^{19}	1.6	37.9	684.4	0.819	21.2	37.9	686.2	0.819	21.3
5 x 10^{19}	0.4	38.2	677.3	0.819	21.2	38.2	679.1	0.819	21.2
1 x 10^{20}	0.4	38.2	670.3	0.818	20.9	38.2	672.2	0.819	21.0

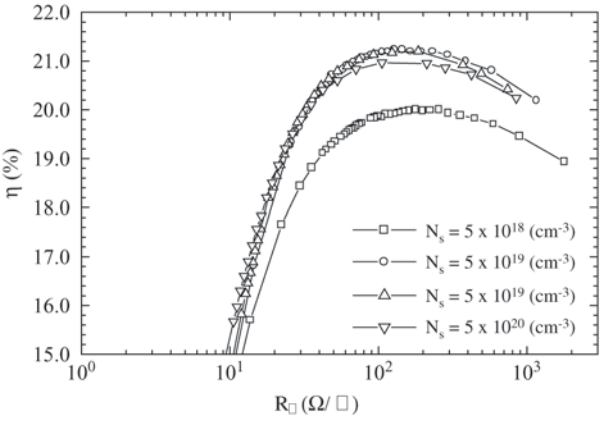

Figure 8. Efficiency, η as function of emitter sheet resistivity, $R_□$ and surface doping level, N_s, considering p-type emitter solar cells.

region and the rear surface recombination velocity were assumed to be null, as mentioned before. Thus, the outuput electrical parameters (short-circuit current density, J_{sc}, open circuit voltage, V_{oc}, and efficiency, η) as function of the emitter sheet resistivity and the surface doping level are shown in Figs. 6-8, respectively.

The short circuit densities, J_{sc}, were obtained taking into account the photogenerated current densities in emitter and base regions, considering the weight factor (1-F_s) correspondent to the illuminated area.

According to this figure, the highest short-circuit densities (approximately $J_{sc} \approx 38.2$ mA/cm^2) are reached for $N_s = 5 \times 10^{19}$ cm^{-3} and $N_s = 1 \times 10^{20}$ cm^{-3}, corresponding to a wide emitter sheet resistivity range $R_□ = (185\text{-}93)$ Ω/□ and $R_□ = (211\text{-}71)$ Ω/□ respectively, despite the highest emitter collection efficiency had been obtained for $N_s = 5 \times 10^{18}$ cm^{-3}, as it was shown in Fig. 5. This fact, as mentioned before, is due to the high shadowing factor, F_s, provided by the moderately doped emitters, correlated to the increase of the metal-semiconductor contact resistivity.

In Fig. 7 it can be observed that the highest open circuit voltage are reached for the sheet resistivity ranges (10-100) Ω/□ and (25-200) Ω/□ corresponding to relatively deep, and moderately doped emitters, ($N_s = 5 \times 10^{18}$ cm^{-3} – 1×10^{19} cm^{-3}), respectively, since they provide the lowest recombination, as it can be seen in Fig. 1.

Thus, as both parameters (short-circuit current density and open-circuit voltage) are competitive, the best surface doping levels are going to be determined by the solar cell efficiencies.

According to Fig. 8, there is a wide range of emitter sheet resistivity (50 – 500 Ω/□) that provides efficiencies around 21%, when the surface doping levels $N_s = 1 \times 10^{19}$ cm^{-3} and 5×10^{19} cm^{-3} are considered; the most efficient P$^+$-type passivated homogeneous emitters correspond to η = 21.2% with the thickness range (1.6 – 0.4) μm.

5. Updating Output Electrical Parameters

In order to evaluate the influence of the recently proposed $n_i = 9.65 \times 10^9$ cm^{-3}, the optimized output electrical parameters (short-circuit current density, open-circuit voltage, fill factor and efficiency) were compared for both values of n_i, as follows in Table 2.

It can be observed that, if the recently proposed n_i is considered, no modification is obtained in the short-circuit current densities, J_{sc}, but there is a slight increase in the V_{oc}, consequently providing a slight increase (≈ 0.1%) in the efficiency, η. These results validate the present conclusions even if small corrections are made in the currently carrier intrinsic concentration $n_i = 1 \times 10^{10}$ cm^{-3} (T = 300 K).

6. Conclusion

Passivated homogeneous p$^+$-type emitters have low emitter recombination ($J_{oe} = 1.2 \times 10^{-13}$ A/cm^2 for $N_s = 1 \times 10^{19}$ cm^{-3} and $R_□ = 145$ Ω/□) and are dominated by the surface recombination component, behaving as transparent emitters for thicknesses up to 3.0 μm.

Gaussian profile p$^+$-type emitters also presented high emitter collection efficiencies, even if they are highly doped and shallow. It was found that only if the optimized emitter sheet resistivities for each surface doping level is consid-

ered, the collection efficiency of the moderated doped emitters are slightly higher than the highly doped ones.

As long as the high quality of p^+-type homogeneous emitters was made evident, p^+nn^+ solar cells optimization was carried out, taking into account the contribution of the optimum metal-grid and shadowing factors to the output electrical parameters (short-circuit current density, open-circuit voltage and efficiency).

It was found that the metal-semiconductor contact resistivity dependence on surface doping level increased the optimum shadowing factor for moderately doped emitters, $N_s = 1 \times 10^{19}$ cm^{-3} and 5×10^{18} cm^{-3}; and therefore, decreasing their short-circuit current densities. On the other hand, the moderately doped emitters also presented the highest open-circuit voltages due to their excellent recombination current densities.

Thus, there is a trade-off between both parameters (short-circuit current density and open-circuit voltage), the maximum efficiencies, $\eta \approx 21.2\%$ were found for the surface doping levels (1×10^{19} - 5×10^{19}) cm^{-3}, emitter thicknesses range (1.6 and 0.4) μm and sheet resistivities (145 – 185) Ω/□, respectively. Another point to stress is that these surface doping levels can provide efficiencies around 21% for a wide range of emitter sheet resistivity (50 – 500 Ω/□).

Although in this work all theoretical optimizations were made considering $n_i = 1 \times 10^{10}$ cm^{-3}, a brief evaluation of the recently proposed value influence ($n_i = 9.65 \times 10^9$ cm^{-3}) on the optimized results showed a non-significant change, validating all present conclusions.

Aknowledgments

This work was supported by FAPESP under contract nº 95/09435-0.

References

1. Cuevas, A.; Merchán, R.; Ramos, J.C. "*Updated contour plots for the design of p⁺ emitters of silicon solar cells*", In Proceedings of the 23rd IEEE Photovoltaic Specialists Conference, IEEE Press, New York, p. 309-314, Conference held in Lousville, K.Y., USA, 1993.
2. King, R.R. "*Studies of diffused boron emitters: saturation current, bandgap narrowing, and surface recombination velocity*", IEEE Transactions on Electron Devices, v. 38, n. 6, p.1399 – 1409, June 1991.
3. Cuevas, A.; Stuckings, M.; Lau, J.; Petravic, M. "*The recombination velocity of boron diffused silicon surfaces*", In Proceedings of 14th European Photovoltaic Solar Energy Conference and Exhibition, Conference held in Barcelona (Catalunya), Spain, 30 June-4 July, 1997.
4. Verliden, P.J.; Sinton, R.A.; Wichkan, K.; Crane, R.A.; Swanson, R.M. "*Backside-contact silicon solar cells with improved efficiency for the '96 World Solar Challenge'* ", In Proceedings of 14th European Photovoltaic Solar Energy Conference and Exhibition, p. 96-99, Conference held in Barcelona, Spain, 30 June – 4 July, 1997.
5. Green, M.A.; Keevers, M.J. "*Optical properties of intrinsic silicon at 300K*", Progress in Photovoltaics, v. 3, n. 3, p. 189-192, May 1995.
6. Green, M.A. *"Solar cells: optimization principles, technology and system applications*", p.78, (Englewood Cliffs: Prentice Hall), 1982.
7. Swirhun, S.E., PhD Dissertation, Stanford University, 1987.
8. Cuevas, A.; Russel, D.A. "*Co-optimization of the emitter region and metal grid of silicon solar cells*", Progress in Photovoltaics, v. 8, n. 6, p. 603-616, 2000.
9. Altermatt, P.P.; Schumacher, J.O.; Cuevas, A.; Glunz, S.W.; King, R.R.; Heiser, G.; Schenk, A. "*The extraction of the surface recombination velocity of Si: P emitters using advanced silicon models"*, In CD-ROM of 16th European PV Solar Energy Conference, Conference held in Glasgow, UK, 1-5 May 2000.